communications biology

Article

https://doi.org/10.1038/s42003-024-07419-4

A BAG-1-inhibitory peptide, GO-Pep, suppresses c-Raf activity in cancer

Check for updates

Ozge Tatli[1,2], Ecenur Cebi[1], Miray Turk[1], Baran Dingiloglu[1], Aycan Sezan[3], Ezgi Basturk[1], Betul Zehra Temur[4], Alp Ertunga Eyupoglu[5], Berna Bicak[6], Esra Erdal[6], Batu Erman[5], Özge Can[7] & Gizem Dinler Doganay[1,8] ✉

BAG-1 interacts with multiple partners, particularly with c-Raf, and promotes cancer cell survival. Hence, modulating the BAG-1-associated interactions with novel inhibitors could provide benefit for cancer therapy. Using HDX-MS, we first demonstrate the higher-order structure of BAG-1S and identify a potential "druggable" site on its BAG domain. An LC-MS/MS-coupled cell-free binding experiment is then used to map the BAG-1S:c-Raf interface, uncovering a 20-amino acid-length region of BAG-1S that is most likely to interact with c-Raf. Site-directed mutagenesis experiments reveal that K149 and L156 are hot spots for BAG-1S:c-Raf interaction, and their substitutions with alanine attenuate the survival of MCF-7 cells. We then show that a peptide derived from the BAG-1S-interacting c-Raf region hinders BAG domain-associated partners. The peptide, engineered with a cell-penetrating peptide motif, can penetrate cells, and it induces apoptosis in cancer cells. The anticancer activity of the peptide might lead to improved treatments for BAG-1-overexpressed and/or MAPK-driven tumors.

BAG-1 is a nucleotide exchange factor related to the molecular chaperone HSP70/HSC70. The anti-apoptotic and prognostic role of BAG-1 has been documented in several human malignancies, such as breast carcinoma[1], hepatocellular carcinoma[2], leukemia[3], lung adenoma[4], neuroblastoma[5] and prostate cancer[6]. BAG-1 expression has also been shown to correlate with drug resistance in several cancer types, suggesting its function as a protector of tumor cell survival upon exposure to anti-tumor drugs[3,7–9].

BAG-1 is expressed as multiple isoforms (-1L, -1M, -1S, -1XS)[10] that assist the assembly of multi-protein complexes engaged in diverse cellular activities including cell proliferation and survival, transcription, apoptosis, and cell motility through their interactions with numerous other proteins. Of these, the interaction of BAG-1 with Raf kinases is particularly critical in relaying signals. Under normal physiological circumstances, c-Raf and HSP70 compete to bind the C-terminal BAG domain of BAG-1[11]. c-Raf is activated upon BAG-1 binding, subsequently triggering the activation of the downstream ERK kinases, thereby promoting either cell proliferation or migration. In cells overexpressing BAG-1, c-Raf, which normally requires Ras for activation, can be activated independently of Ras through BAG-1 binding[11]. Thereby, designing small compounds, inhibitors, or peptides that impede the assembly of the BAG-1:c-Raf complex may effectively suppress tumor development and/or progression by targeting the prolonged survival and high proliferation capacity of malignant cells. In many human cancers, tumor growth and drug resistance are driven by the aberrant activity of Raf proteins, particularly B-Raf and c-Raf. Although B-Raf has garnered the greatest interest owing to its high incidence of mutations, the role of c-Raf in carcinogenesis and drug resistance is increasingly gaining clinical relevance[12]. For instance, c-Raf expression in basal-like breast cancer is associated with a more aggressive phenotype and a poor survival rate[13]. Moreover, multiple studies demonstrate that Ras-driven cancers develop a dependency on c-Raf expression for the activation of the MAPK pathway[14]. Similarly, growing evidence reveals that c-Raf is a key player in promoting therapeutic resistance to MAPK-targeted therapies[14]. Therefore, the BAG-1S:c-Raf interaction is a promising therapeutic target in BAG-1 over-expressed and/or in MAPK-activated cancer types.

Our research endeavors to develop new inhibitors targeting the molecular co-chaperone BAG-1 with a particular emphasis on its c-Raf

[1]Molecular Biology-Genetics and Biotechnology, Graduate School, Istanbul Technical University, Istanbul, Türkiye. [2]Department of Molecular Biology and Genetics, Faculty of Engineering and Natural Sciences, Istanbul Medeniyet University, Istanbul, Türkiye. [3]Department of Biology, Institute of Natural and Applied Sciences, Cukurova University, Adana, Türkiye. [4]Department of Medical Biotechnology, Institute of Health Sciences, Acibadem University, Istanbul, Türkiye. [5]Department of Molecular Biology and Genetics, Graduate School of Natural and Applied Sciences, Acibadem University, Istanbul, Turkey. [6]Izmir Biomedicine and Genome Center, Faculty of Medicine, Dokuz Eylul University, Izmir, Türkiye. [7]Department of Biomedical Engineering, Faculty of Engineering and Natural Sciences, Acibadem University, Istanbul, Türkiye. [8]Department of Molecular Biology and Genetics, Faculty of Arts and Science, Istanbul Technical University, Istanbul, Türkiye. ✉e-mail: gddoganay@itu.edu.tr

interaction. Given this, we searched for the binding sites and 'hotspots' of the BAG-1S:c-Raf complex and explored the inhibitory activity of a peptide derived from the natural amino acid sequences that mimics interactor proteins. We successfully identified a peptide capable of modulating BAG domain-associated complexes of BAG-1S. When combined with a cell-penetrating sequence, the peptide exhibited a potent cell growth suppression activity against cancer cells. Herein, we describe the pipeline from the discovery of the interaction surface of the BAG-1S:c-Raf complex to designing and characterizing a candidate lead peptide, GO-Pep, aspiring to contribute to improved treatment strategies.

Results

Druggability profile of BAG-1S

To describe the 3D protein surface structure of the full-length human BAG-1 protein, we adopted a hydrogen-deuterium exchange mass spectrometry (HDX-MS)-guided structural study. We used the sequence of the most abundant isoform, cytosolic BAG-1S, which is 230 amino acids in length. Leveraging a TEV digestion site placed after an N-terminal polyhistidine tag, BAG-1S was purified through a tandem Ni-NTA purification strategy (Fig. S1A, B). Purified BAG-1S was in a monomeric state with a dominant α-helical structure (Fig. S1C, D). For HDX experiments, BAG-1S was incubated in deuterated buffer up to 200 min, and the deuterium incorporation rates of peptic peptides were analyzed by DynamX (Fig. 1A). HDX-MS data enabled the identification of 114 peptides, accounting for 98.7% sequence coverage (Fig. S2A). Color-coded peptide-specific deuterium incorporation rates were projected onto the BAG-1S structure, and deuterium uptakes were traced over time (Fig. S2B, Fig. 1B). Relative isotope incorporation of different peptide regions was depicted as Woods plots for all time points (Fig. 1C). The three-helix bundle BAG domain showed a more solvent-protected and stabilized structure compared to the ubiquitin-like (UBL) domain. Intriguingly, HDX data unveiled a segment on the BAG domain corresponding to residues between 136 and 160 of BAG-1S that exhibited a solvent-protected site surrounded by dynamic regions. In parallel, the peptide NKELTGIQQGFLPKDL (136-153 amino acids, +2 charge) displayed bimodal HDX kinetics, implying the occurrence of two isotopic envelopes interconverted by slow dynamics (Fig. 1D). The exchanging

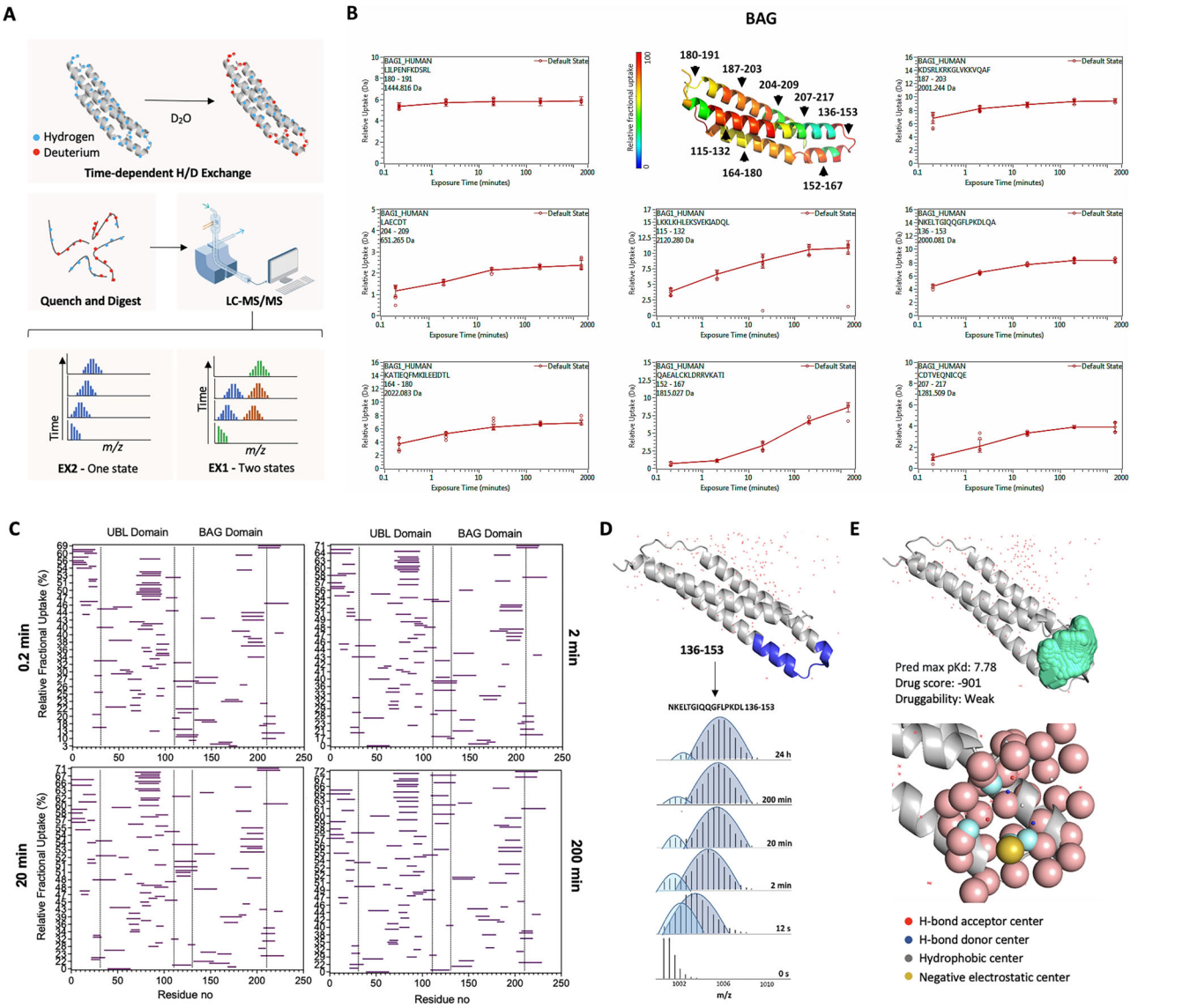

Fig. 1 | Druggability profile and surface character of BAG-1S. A Workflow for an HDX-MS experiment. The mass distributions that arise from the HDX–MS experiment for a peptide that exists in one conformation (EX2) or two separate conformations (EX1). **B** Time-dependent relative deuterium uptake of representative peptides on BAG domain (Chain B from 1HX1). The data are depicted as relative deuterium uptake versus time on a logarithmic scale. ($n = 2$) **C** Relative deuterium incorporation of BAG-1S peptides represented by Woods plots. **D** Mass spectra of BAG domain peptide of NKELTGIQQGFLPKDL (136-153 amino acids, +2 charge) that show bimodal HDX kinetics. **E** CavityPlus analysis of BAG-1 showing an internal cavity. Figures were drawn with PyMOL (http://pymol.org).

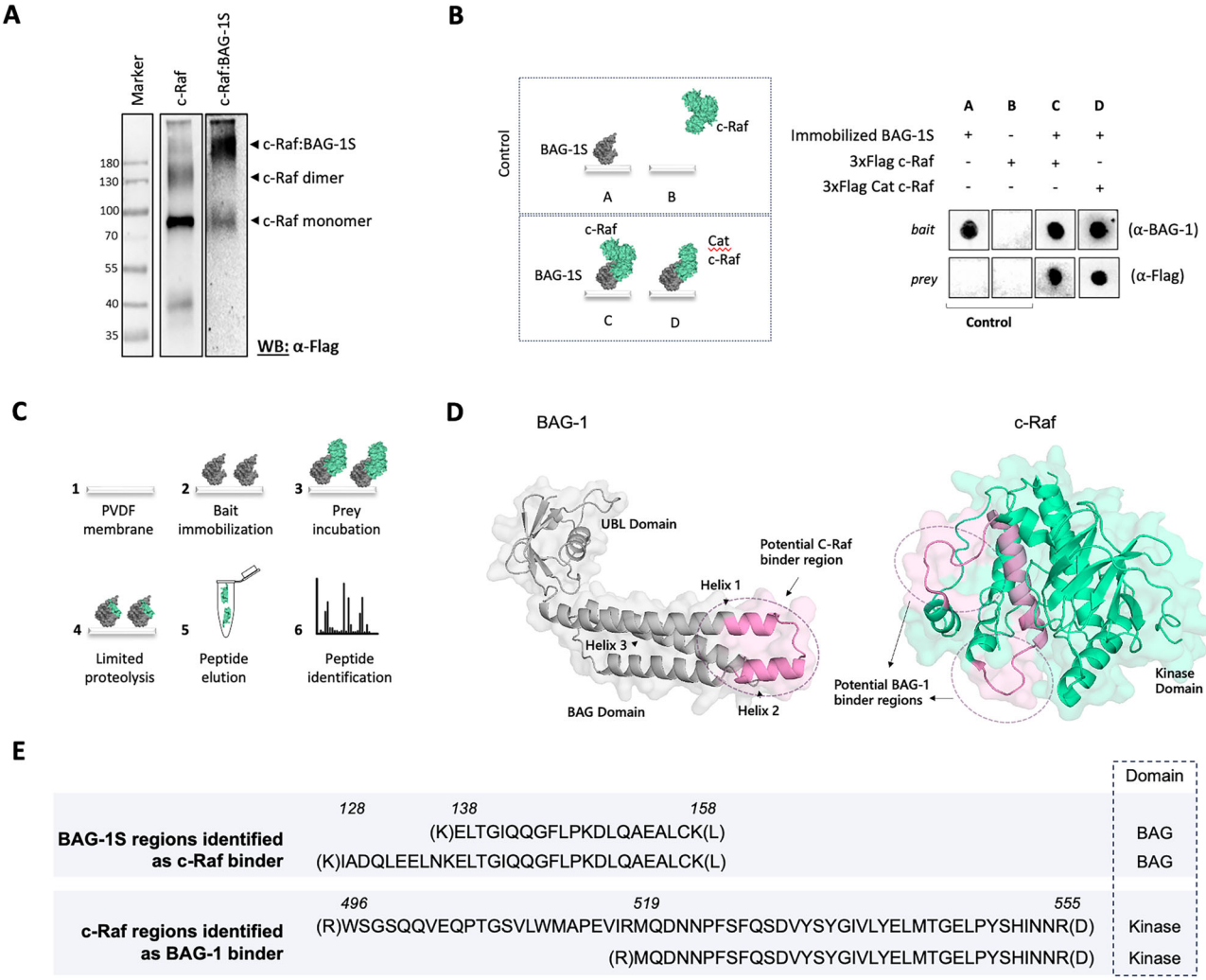

Fig. 2 | Identification of a plausible BAG-1S:c-Raf interaction site. A In vitro cross-linking analysis of affinity purified 3xFlagc-Raf in the presence and absence of BAG-1S. Cross-linked samples were subjected to immunoblotting. The position of monomers and crosslinked dimers are indicated. **B** Schematic depiction of in vitro binding assay and immunoblots for the binary interaction of BAG-1S with affinity-purified full-length 3xFlagc-Raf or catalytic domain of 3xFlagc-Raf. **C** Schematic depiction of in vitro binding assay coupled to LC-MS/MS for the identification of interacting peptides. Following limited proteolysis of preformed complexes, peptides eluted were analyzed by mass spectrometry. **D** Identified regions are shown on the BAG-1 and c-Raf structures. Gray: BAG-1, Green: c-Raf (3OMV), Pink: predicted interaction regions. **E** Peptide sequence of identified binding regions and their domain origin.

populations of this peptide completed deuteration in 24 h. CavityPlus[15] analysis revealed a predicted cavity (area, 276.25 Å^2; volume, 377.88 Å^3; number of residues, 24), which was aligned with the region identified via HDX-MS. However, the calculated Pred max pKd score predicted that this site was a relatively weak druggable region (Fig. 1E). These findings suggest that this particular region on the BAG domain has the potential to function as a druggable binding pocket capable of accommodating presumably a peptide rather than a small molecule.

Interaction surfaces of BAG-1S:c-Raf complex

BAG-1:c-Raf interaction has been previously established by pull-down experiments[11], however, there are currently no accessible structures of BAG-1 complexed with c-Raf in the PDB database. To examine whether BAG-1S:c-Raf interaction might serve as a potential protein-protein interface target, we first sought to locate the contact regions of the complex. To verify this interaction, a BAG-1S:c-Raf complex was obtained by incubating affinity purified BAG-1S and 3xFlag c-Raf proteins in vitro and further chemically cross-linked using a non-cleavable mid-length crosslinker, disuccinimidyl suberate (DSS). Both proteins were in a monomeric state before complex formation. When chemically cross-linked with DSS, the formed complex yielded a molecular weight greater than 200 kDa, revealing that BAG-1S might trigger dimerization of the c-Raf protein in vitro (Fig. 2A). To further map the interface of the binary BAG-1S:c-Raf complex, an on-membrane in vitro binding assay was carried out. We first confirmed the in vitro interaction on the membrane using BAG-1S as a bait and the epitope-tagged full-length c-Raf or the kinase domain of c-Raf as a prey (Fig. 2B). As a negative control, immobilized BAG-1S was incubated with an anti-Flag antibody in the absence of c-Raf. We verified the binding of BAG-1S to the kinase domain of c-Raf (Fig. 2B), which was evidenced previously[11]. To further identify interacting regions, preformed BAG-1S:c-Raf complexes were subjected to limited trypsinolysis. BAG-1S binder c-Raf peptides or c-Raf binder BAG-1S peptides were acid-eluted, enriched, and analyzed by mass spectrometry (Fig. 2C). As a negative control, BAG-1S only and c-Raf only samples were also subjected to the same experimental workflow and analyzed accordingly. No peptide was detected in the control membranes. Two peptide sequences from the BAG domain of BAG-1S were identified as c-Raf binders and contained a 20-amino acid overlapping sequence. Similarly, two peptide sequences from the kinase domain of c-Raf were identified as BAG-1S binders and included a 36-amino acid overlapping sequence. These regions were mapped onto the structures of BAG-1 and c-Raf and shown in pink (Fig. 2D). Thus, peptides derived from the BAG domain showed the region where BAG-1S interacts with c-Raf, whereas those

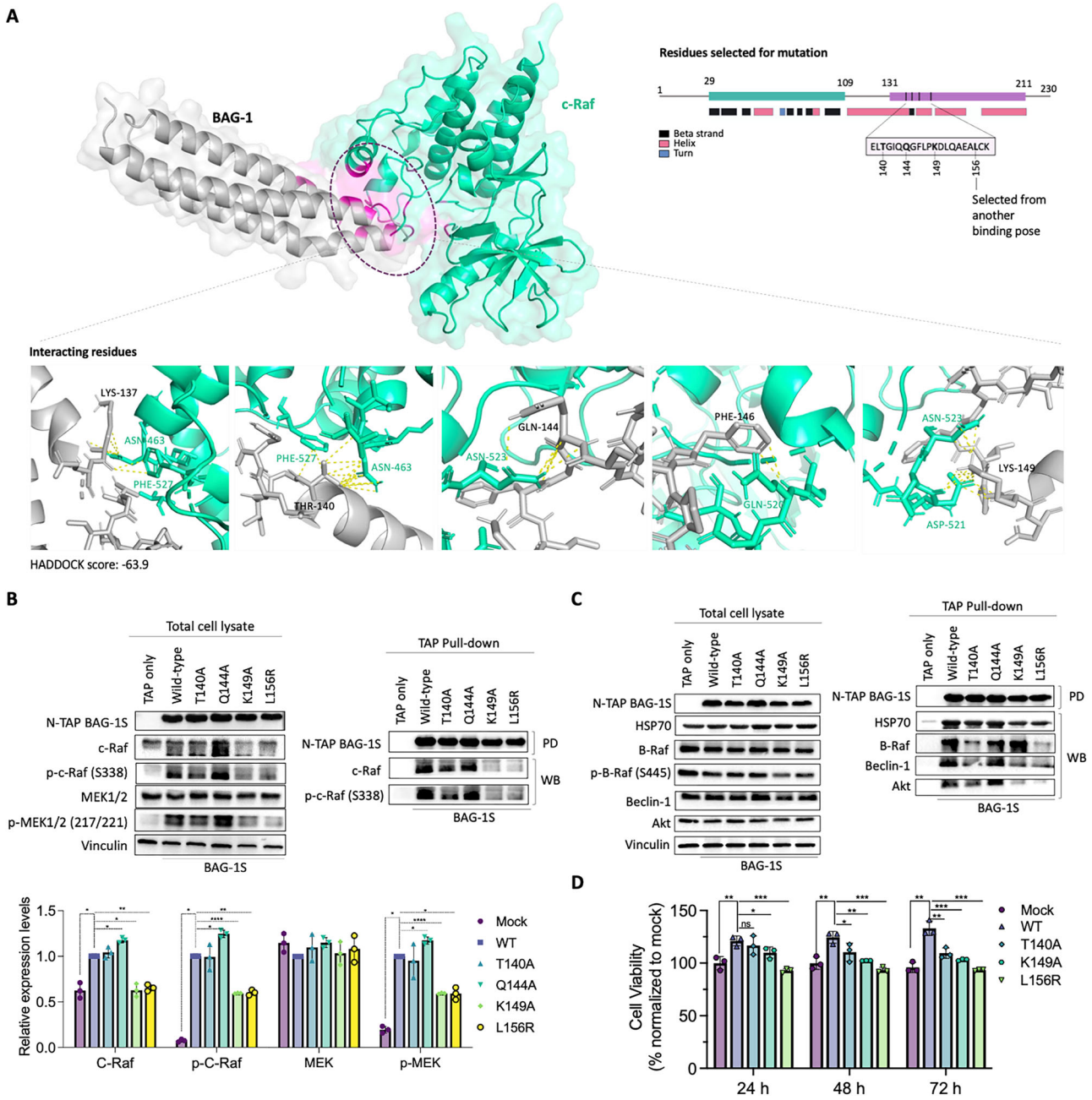

Fig. 3 | The Bag-1S:c-Raf interaction is mediated by T140/K149/L156 residues in the BAG domain of BAG-1S. A A cartoon representation of BAG-1:c-Raf interaction upon molecular docking. Potential interacting residues were shown as sticks. The regions shown in pink indicate potential interaction regions. Gray: BAG-1 (1HX1), Green: c-Raf (3OMV). Location of interacting residues were depicted on amino acid sequence of BAG-1S. Mutated amino acids were shown as bold. **B** The effect of the over-expression of WT BAG-1S and its mutant forms on intracellular c-Raf, p-c-Raf (S338), p-MEK (217/221) levels. MCF-7 cells were transfected with an empty vector (control) containing only the TAP sequence, wild-type BAG-1S (wild-type), or mutant plasmids T140A, Q144A, K149A, L156R of BAG-1S. Expression levels and phosphorylation status of endogenous MAPK components dependent on BAG-1S expression were tested by immunoblotting. Expression levels were normalized with the Vinculin levels and then analyzed by *t*-test. Interactions were analyzed by TAP pull-down experiments. ($n = 3$) Error bars indicate standard deviation (SD). **C** Investigation of the interaction of WT BAG-1S and its mutant forms with other BAG-domain intracellular interaction partners of BAG-1S by TAP pull-down. **D** Effect of BAG-1S mutations on proliferation of MCF-7 cells. Cell viability assessed by MTT assay for 24, 48 and 72 h post-transfection. Then, the percentage of cell viability was determined by normalizing the absorbances of BAG-1S transfected cells to those of empty vector transfected cells. ($n = 3$) Control: only TAP control. WT: Wild-type BAG-1S. $^{*}p \le 0.05$, $^{**}p \le 0.01$, $^{***}p \le 0.001$, $^{****}p \le 0.0001$. Error bars indicate standard deviation (SD).

identified from the catalytic c-Raf domain revealed the region where c-Raf interacts with BAG-1S (Fig. 2E).

Fine mapping c-Raf-interacting BAG-1 site by mutations

To pinpoint the specific residues involved in the formation of their structural complex, we carried out an in silico site-directed molecular docking approach employing HADDOCK using available structures in the PDB (BAG domain: 1HX1 (X-Ray) and c-Raf kinase domain: 3OMV (NMR)). The active residues for BAG-1S and c-Raf were designated from MS-guided identified regions. In some of the top poses with the lowest docking energy score, the amino acids located at the binding interface in the models, which coincide with the experimentally detected regions, were found to occupy the BAG-1:c-Raf binding site. Binding affinity of the representative pose (Fig. 3A) was calculated using PRODIGY software[16] as −9.3 kcal/mol (K_D,

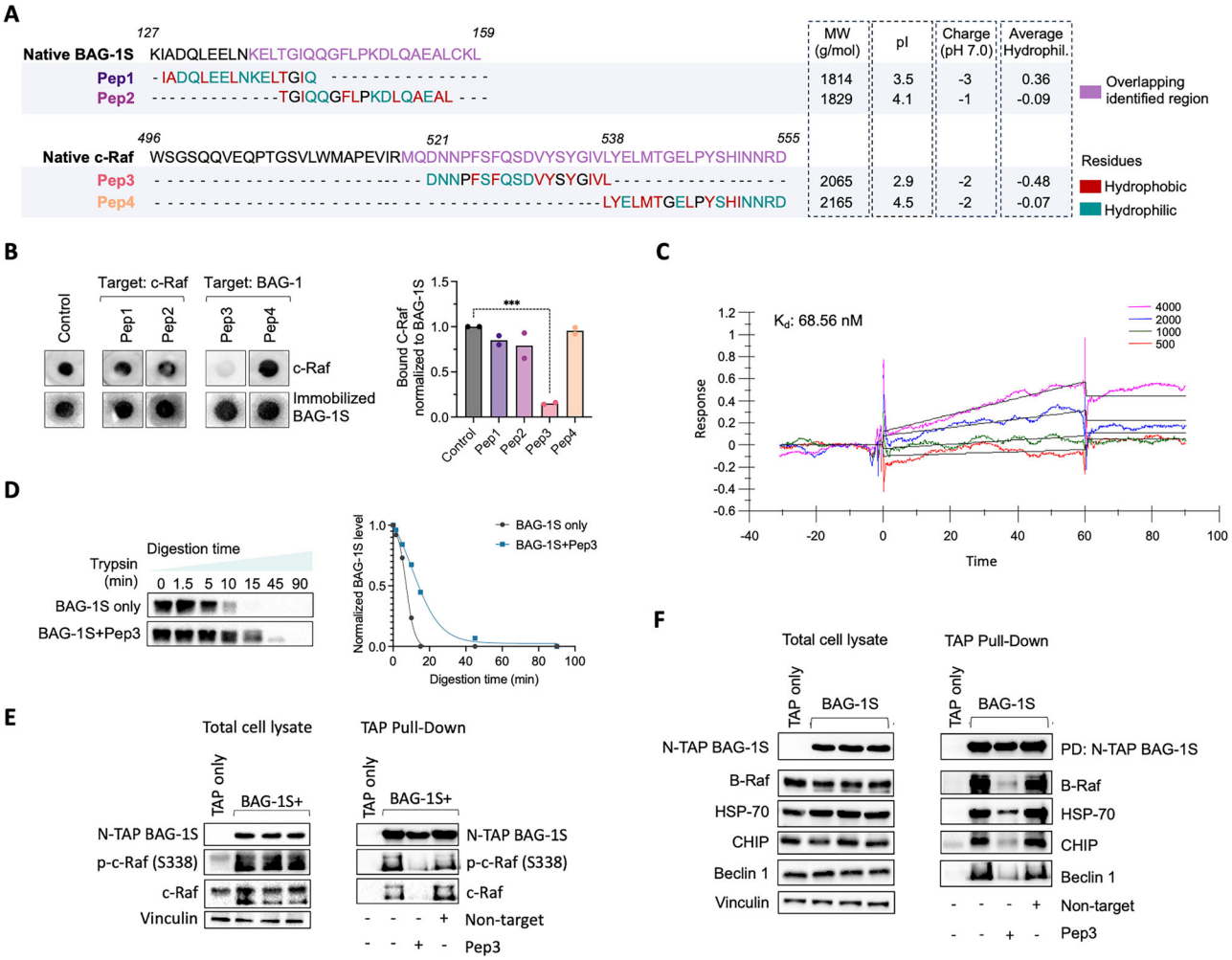

Fig. 4 | Pep3 binds to BAG-1S and disrupts BAG domain-associated complexes. **A** Peptides derived from native BAG-1S and c-Raf interaction region. **B** Screening possible peptides by a competition binding assay ($n = 2$) **C** Testing Pep3 binding via SPR **D** Immunoblots depicting the stability of BAG-1S upon Pep3 binding by limited trypsinolysis as singlet to complement in vitro binding experiments. **E** Testing the activity of Pep3 on BAG-1S:c-Raf interaction. TAP pull-down of BAG-1S was followed by the incubation of precipitated complexes with Pep3. **F** Testing the activity of Pep3 on BAG domain-associated interactions with representative blots of three biological replicates.

1.4×10^{-7} M). Non-covalent interactions were analyzed by using the Protein-Ligand Interaction Profiler (PLIP) software[17]. Three types of interactions were identified upon docking: H-bonding (K137, Q144, K149), hydrophobic interactions (T140, F146) and a salt bridge (K149). Next, ANCHOR web server was employed to identify "hotspot" residues in the complex[18]. Accordingly, BAG-1S K149 (−8.5 kcal/mole) and c-Raf D521 (−6.5 kcal/mole) are indeed hotspot anchors that have been exploited on the design of compounds that bind to these proteins. To experimentally identify hotspot binding residues, single amino acid substitutions were made, with polar or charged residues replaced by alanine residues and nonpolar residues replaced by a charged residue. The residues were selected on the basis of the assessment of multiple poses. These included T140A (α1), Q144A (α1), K149A (loop), and L156R (α2) mutations at the c-Raf binder region of BAG-1S. Next, we addressed whether c-Raf undergoes Ser338 phosphorylation upon mutations on c-Raf interacting site of BAG-1S. Indeed, transfected wild-type BAG-1S markedly elevated the phosphorylation of c-Raf at Ser338 and MEK1/2 at Ser217/221, and this signal increase was abolished for K149A and L156R BAG-1S mutants in MCF-7 cells (Fig. 3B). To assess whether these BAG domain mutations would disrupt the integrity of associated biochemical complexes, we performed TAP pull-down experiments. Figure 3B, C shows the immunoblotting results performed on the elution fractions. BAG-1S-associated c-Raf was monitored in the precipitates of wild-type and mutant BAG-1S proteins, indicating that the T140A mutant displayed a weaker binding to c-Raf, whereas the K149A and L156R mutants, but not Q144A, almost completely abrogated the formation of the BAG-1S:c-Raf complex (Fig. 3B). These findings demonstrated that the BAG-1S:c-Raf interaction is dependent on the BAG-1S K149 and L156 residues, and T140 residue contributes to the binding affinity of the complex. Q144 residue does not seem to be essential for the BAG-1S:c-Raf interaction. Notably, these mutations also affected the formation of other BAG domain-associated interactions of BAG-1S, including HSP70, B-Raf, Beclin 1[19], and Akt (Fig. 3C). To probe whether these mutations suppress the in vitro proliferation of the human breast cancer cells, we carried out an MTT assay on MCF-7 human breast cancer cells. In cells transfected with the BAG-1S T140A, K149A, and L156R mutants, cell viability was relatively lower than that of the cells over-expressing wild-type BAG-1S (Fig. 3D). This observation was statistically significant for all three mutations at 72 h following the transfection.

Identification of a peptide disrupting BAG domain-associated complexes of BAG-1S

We tested the binding activity of peptides by a competition assay with the corresponding partner protein. Four potential modulator peptides were generated from native sequences located on the putative contact surfaces of the BAG-1S:c-Raf complex. Peptide lengths were restricted to 17-18 amino acids (Fig. 4A). Peptides derived from the binder sequences were

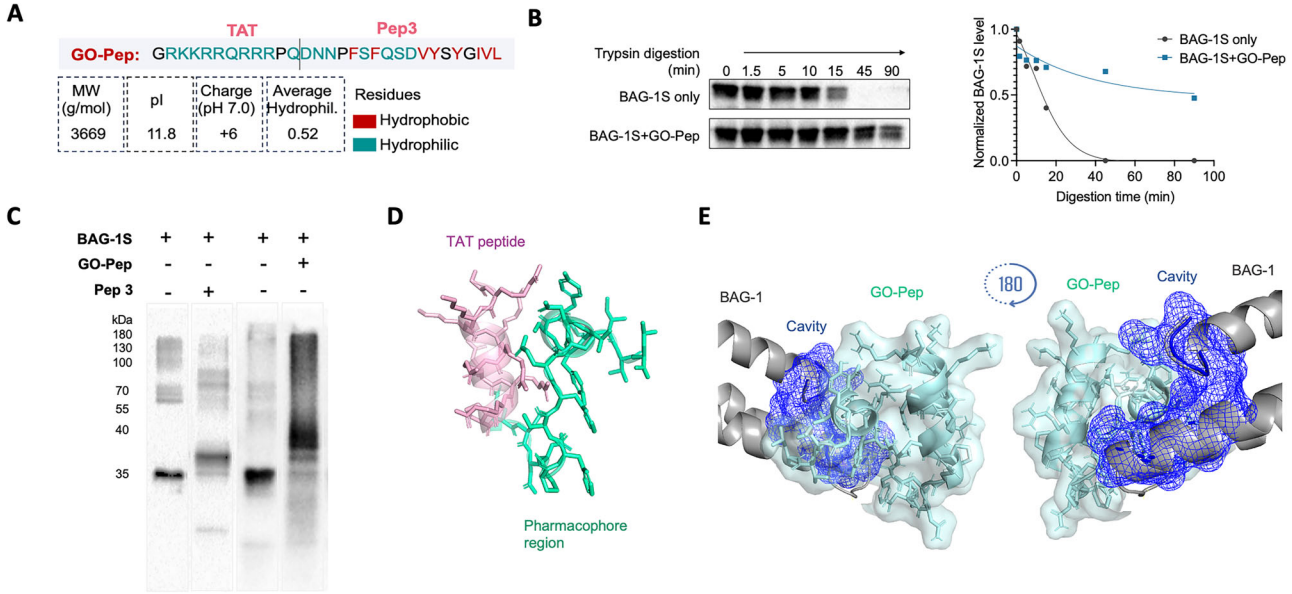

Fig. 5 | GO-Pep binds to BAG-1S. A Peptide sequence and characteristics of GO-Pep. **B** Immunoblot depicting the stability of BAG-1S upon GO-Pep binding by limited trypsinolysis as singlet to complement binding experiments. **C** A representative crosslinking experiment of two biological replicates for Pep3:BAG-1S and GO-Pep:BAG-1S interaction. **D** Predicted three-dimensional structure of GO-Pep modeled by PepFold3 **E** Molecular docking of GO-Pep and BAG-1 performed by HADDOCK server. A stabile interaction between GO-Pep and BAG-1 upon docking was depicted along with the mesh representation of the cavity on BAG domain.

synthesized by employing Fmoc chemistry and further characterized using LC-MS/MS. Both "theoretical" masses and "empirical" masses were determined to be almost identical (Fig. S3). Their potential to inhibit the interaction between BAG-1S and c-Raf was examined experimentally through an in vitro competition binding assay. Of the four peptides tested, Pep3 (net charge: -2), derived from the c-Raf kinase domain, was able to inhibit the binding of c-Raf to BAG-1S, whereas the formation of a BAG-1S:c-Raf complex was not affected by an equivalent concentration of other peptides (Fig. 4B). In the following SPR experiments, Pep3 showed a nanomolar affinity to BAG-1S (K_d: 68.56 nM) (Fig. 4C). Next, we analyzed the stability of the bound complex by limited proteolysis. Pep3 binding enhanced the stability of BAG-1S upon limited trypsinolysis (Fig. 4D). To further assess the ability of Pep3 to impair preformed BAG-1S:c-Raf interaction, TAP (tandem affinity purification)-tagged BAG-1S was pulled down from MCF-7 cell lysates by IgG Sepharose beads. Precipitated BAG-1S-associated complexes were incubated with Pep3 or a non-target peptide diluted in wash buffer for 30 min at 37 °C. Pep3 disrupted the BAG-1S:c-Raf interaction, whereas the interaction was retained in both control sample (no peptide treatment) and non-target peptide-incubated sample under the same experimental conditions (Fig. 4E). Then, the presence of BAG domain-associated interaction partners of BAG-1S was analyzed in TAP-tagged BAG-1S precipitates upon peptide incubation. Accordingly, Pep3 not only hampered c-Raf binding but also efficiently disrupted other BAG domain-associated interactions of BAG-1S, which include Beclin 1, B-Raf, CHIP, and to a lesser extent, HSP70 (Fig. 4F).

Next, we sought to test whether Pep3 treatment could inhibit the proliferation of cancer cells. However, Pep3 is incapable of crossing the lipid bilayer membrane owing to its unfavorable charge and size[20]. Pep3 does not have any Arg or Lys residues that could ease its cellular penetration[21]. Using the webserver BChemRF-CPPred[22], we also computationally affirmed the lack of its cell penetration potential. Unfortunately, Pep3 is devoid of a water-soluble character as well. Therefore, in an effort to achieve membrane permeability and water solubility, a CPP motif including the TAT sequence was combined with the peptide and referred to as GO-Pep (Fig. 5A). As shown by the limited trypsinolysis analysis of BAG-1S with or without GO-Pep, ligand-bound BAG-1S was cleaved at a slower rate than free BAG-1S, indicating the enhanced stability of BAG-1S upon GO-Pep binding (Fig. 5B). Unfortunately, SPR experiments with GO-Pep were unsuccessful due to an excess of non-specific binding of the peptide to the chip. To demonstrate that the GO-Pep retained BAG-1S binding activity, we confirmed BAG-1S:GO-Pep binding through chemical crosslinking experiments (Fig. 5C). The three-dimensional structure of GO-Pep was modeled by PepFold3 server[23] prior to docking experiments (Fig. 5D). Following docking experiments, binding affinity of one of the strongest poses (Fig. 5E) was calculated by PRODIGY software as -7.1 kcal/mol (K_D, 5.8×10^{-6} M). The chemical stability of GO-Pep in PBS was also analyzed. The peptides were incubated at 37 °C for different time periods (up to 4 h), and the integrity of the peptide was then monitored by mass spectrometry. GO-Pep remained intact for up to at least 4 h or after 3 freeze-thaw cycles, and possessed good stability under these experimental conditions (Fig. S4).

Identification of anticancer activity of GO-Pep against human breast and hepatocarcinoma cells

To evaluate the antiproliferative properties of GO-Pep on cancer cells, we performed an MTT cell viability assay on three available cancer cell lines, including MCF-7, SNU-387, and HUH-7 cells. We first tested the effect of TAT peptide in MCF-7 breast cancer cells, utilizing a TAT control peptide for comparison (Fig. 6A). While the GO-Pep significantly decreased the cell viability in a concentration dependent manner, TAT-only peptide did not affect the viability of the cells. Similarly, the treatment of GO-Pep resulted in significant decline in cell viability in hepatocellular carcinoma cells (Fig. 6B). Interestingly, the antiproliferative effect of the peptide was more prominent in SNU-387 cells harboring the N-Ras Q61K mutation (Fig. 6B). To assess whether the cytotoxicity of GO-Pep is specific to cancer cells, the effect of the peptide was assessed on BEAS2b non-tumorigenic lung epithelial cell line and HEK-293T embryonic kidney cells. GO-Pep was potent against cancer cells, but not against normal mammalian cells at the same concentrations (Fig. 6C). To evaluate the selectivity of the peptide, we have investigated the effect of the peptide on BAG-1 knock-out MCF-7 cells by comparing it with a control peptide (TAT only). BAG-1 knockout MCF-7 cell line has been generated and characterized previously[24]. We confirmed the loss of BAG-1 expression by western blot prior to cell viability experiments (Fig. S5). Up to 300 μM, we could not discern a substantial difference between the effects of GO-Pep and the control peptide. In comparison to

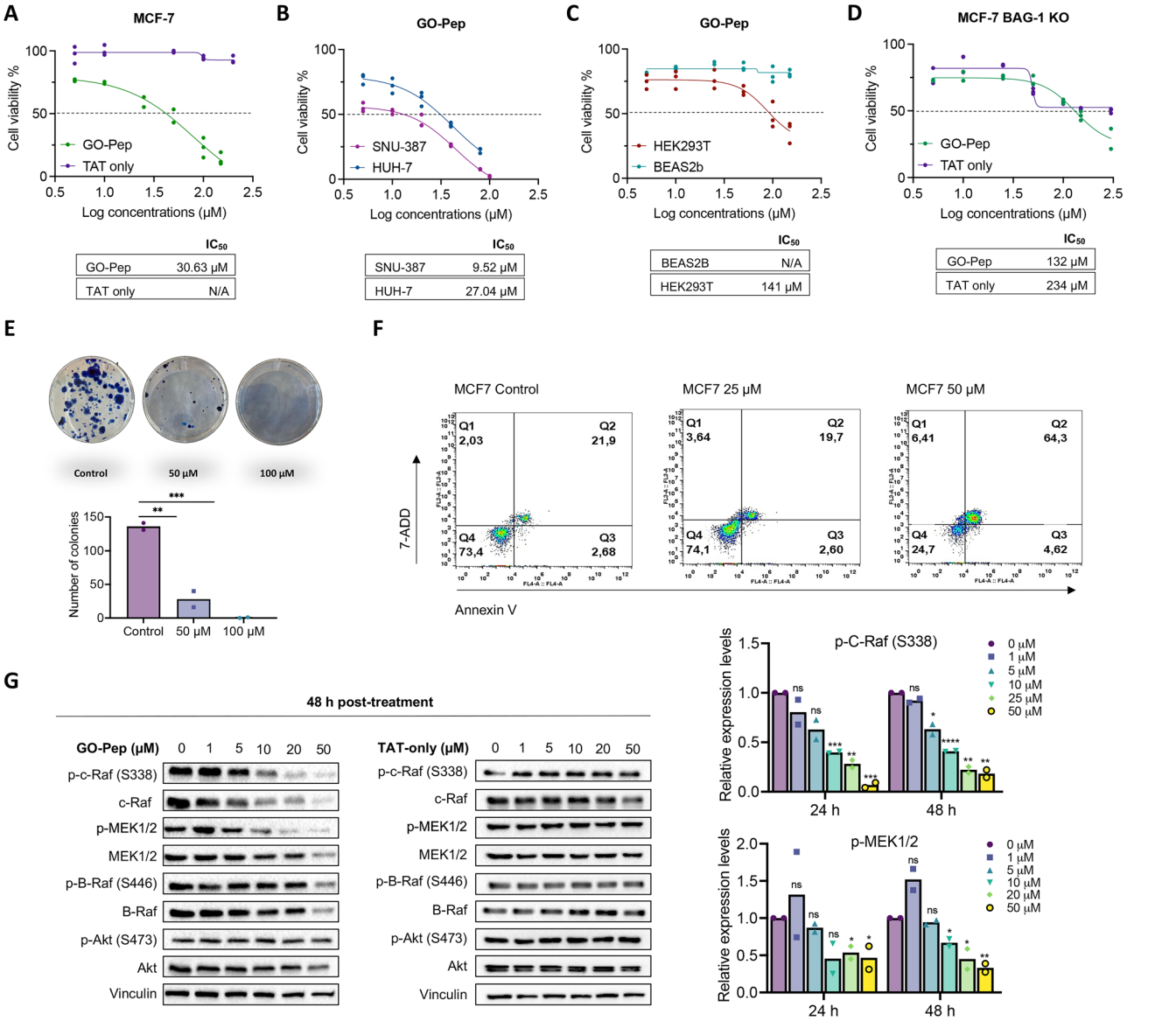

Fig. 6 | Anticancer activity of GO-Pep. A MTT assay to determine the effect of GO-Pep and TAT-only on the viability of MCF-7 breast cancer cells. **B** Anticancer activity of GO-Pep in SNU-387 and HUH-7 HCC cells. **C** Cytotoxicity of GO-Pep on HEK293T and BEAS2b cells. **D** The effect of GO-Pep and TAT-only on the viability of MCF-7 breast cancer cells. **E** Clonogenic cell survival assay showing representative images of the colonies formed in control and MCF-7 cells following treatment with the indicated concentrations of GO-Pep. Colonies were quantified ($n = 2$) **F** FL3-A channel 7-AAD; FL4-A channel refers to Annexin V. Apoptotic cell rates in MCF-7 cells treated with GO-Pep and PBS as a control. Apoptosis ratio was measured by flow cytometry. The late and early right quadrants show the apoptotic cell population. Two different doses were administered as 25 μM and 50 μM. **G** Immunoblotting analysis to define the effect of different concentrations of GO-Pep and TAT-only peptide control on the expression of MAPK signaling genes in MCF-7 cells. Vinculin is used as a loading control. ($n = 2$) $p > 0.05$(n.s.), $p \le 0.05$(*), $p \le 0.01$(**), $p \le 0.001$(***), $p \le 0.0001$(****).

wild type MCF-7 cells, the inhibitory effect of GO-Pep on the survival of the MCF-7 cells was significantly attenuated in the absence of BAG-1 isoforms (Fig. 6D). Next, the clonal expansion of MCF-7 cells after treatment with GO-Pep was evaluated by a colony formation assay (Fig. 6E). In colonies compared to the vehicle-treated control, 50 and 100 μM GO-Pep treatment significantly inhibited colony formation in a dose-dependent manner ($p < 0.01$). To ascertain whether GO-Pep treatment would cause apoptosis, we treated MCF-7 cells with 25 and 50 μM of peptide and analyzed the cells by flow cytometry. We found that GO-Pep application induced a notable increase in the number of apoptotic cells. After 48 h incubation with 50 μM peptide, the late apoptotic cell population was dramatically increased to 64.3% as compared with control cells (21.9%) (Fig. 6F). We further investigated the effect of GO-Pep on the phosphorylation level of c-Raf and MEK1/2 in MCF-7 cells. Western blot analysis revealed that GO-Pep selectively suppressed the phosphorylation of c-Raf (Ser338) and MEK1/2 (Ser217/221) at a concentration of 10 μM following 48 h of peptide incubation. To rule out the possibility that CPP peptide would interfere with the MAPK pathway, TAT peptide only was used as a control, and displayed no significant alteration in the MAPK pathway at the same concentrations in MCF-7 cells (Fig. 6G). These findings also demonstrate that GO-Pep enters cells, binds to BAG-1S and subsequently inhibits the BAG-1S:c-Raf interaction, thereby impeding the activity of the downstream effector protein, MEK1/2, and decreasing cell proliferation.

Discussion

In MAPK-driven cancer entities, c-Raf is becoming more recognized as a critical player in promoting drug resistance[14]. Substantial evidence also suggests that certain Ras-driven cancers develop addiction to c-Raf

signaling[12,25–27]. Both c-Raf and BAG-1 have been implicated to play a role in drug resistance and have a prognostic value for cancer[2,8,28–30]. Encouraged by these, we explored the interaction between BAG-1 and c-Raf, an aspect that exhibits promise as a potential protein-protein interaction (PPI) target for therapeutic intervention.

To selectively alter PPIs, first, it is important to identify 'druggable' regions on proteins that might be amenable to small-molecule or peptide inhibition. Druggable regions can accommodate inhibitor binding to directly blockade a specific PPI. Leveraging HDX-MS, we here identified a solvent-protected embedding region on BAG domain, which features a pocket-like conformation in the transition site from the 1st to the 2nd helix, as well as a stretch surrounded by surface exposed amino acids. In such structures, the solvent-protected rigid region acts as a stable binding segment for the ligand, with the surrounding flexible components providing support to position the ligand to the binding site, implementing the determined site on BAG domain to be a probable druggable site. When we exploit the BAG-1S interacting c-Raf region, the determined interaction surface (helices 1 and 2 linked by a loop region on BAG domain) overlapped with our HDX-MS predicted druggable site. Druggable sites typically comprise a cluster of binding hotspots, therefore, we investigated whether this region harbors hotspot residues involved in c-Raf binding. Specifically, two main residues (K149 in the loop, L156 in α2) on BAG domain were found to be the major contributors to the BAG-1S:c-Raf interaction. In vitro binding experiments have identified this region as the site of c-Raf interaction, however, we cannot rule out the possibility that L156R mutation might induce a structural alteration in the BAG-1 protein and indirectly affect c-Raf binding. Yet, the region we identified coincides with the region that was previously shown for c-Raf binding with the truncated forms of BAG-1[11]. According to the same study, BAG-1:c-Raf interaction requires helices 1 and 2 of BAG domain, and c-Raf and HSP70 compete for the helix 2 region of BAG domain. In a prior study performed to investigate druggable sites on BAG-1L, Cato et al. has also offered that BAG-1 possesses a groove comprised of helix 1 and 2 residues of K231/232/279 A (K116/117/164 corresponding BAG-1S residues) for the binding of Androgen Receptor (AR), which was found to be suitable for peptide or peptide-mimetic modulators[6]. Nevertheless, the position of the groove residues varies between the two findings with a minor overlap, suggesting alternate target surfaces for intervention, either for the choice of recruited signaling cascade variations or isoform-specific alterations in function.

Our findings on the contact surfaces led us to design a peptide, Pep3, to disrupt the BAG-1S:c-Raf complex, targeting the identified c-Raf binder region of BAG-1S. Pep3 drastically altered the binary interaction of c-Raf with BAG-1S. We therefore affirmed that this region on c-Raf is responsible for BAG-1 binding and serves as a target surface for future drug design studies. It has been previously reported that BAG-1S mediates the stabilization of a set of specific pro-survival proteins, which also includes c-Raf, and enhances the survival of osteosarcoma cells expressing oncogenic MYC[31]. Our study showed that the disruption of BAG-1S:c-Raf interaction decreased the cellular levels of both p-c-Raf and c-Raf in both BAG-1 mutants and Pep3-treated BAG-1 complexes. This reinforces the notion that BAG-1 might stabilize c-Raf structure, rendering it a viable target to inhibit c-Raf activity in cancer. Pep3 also deployed several BAG domain-associated interactions of BAG-1, including HSP70, Beclin 1, CHIP and B-Raf. Pep3 may potentially diminish the partners of other BAG-1 isoforms, each possessing an evolutionarily conserved BAG domain at their C-terminus. All these partners are critical players involved in different cell survival pathways[11,12,19,32]. Of these, the loss of Beclin 1 interaction is quite intriguing and requires more research since the precise role of autophagy in cancer is yet obscure[19]. Given that HSP70/Hsc70 and CHIP interactions of BAG-1 were disrupted following Pep3 incubation, it is very likely for the peptide to also interfere with the action of the other heat shock protein family members, including GRP78 (BiP) and GRP75 (mortalin), which have been linked to processes including endoplasmic reticulum stress and mitochondrial biogenesis[33,34]. The capacity of Pep3 to impair various interactions of BAG-1 associated with distinct cell survival pathways broadens its potential use to inhibit the survival of cancer cells.

To assess the anticancer properties of Pep3 identified in our hands, we combined it with a cell-penetrating peptide (CPP) motif and generated a peptide, GO-Pep, which inhibited proliferation of MCF-7, SNU-387, and HUH-7 cancer cells by suppressing BAG domain-associated interactions of BAG-1. We have previously demonstrated an important disparity in growth between control and BAG-1 CRISPR/Cas9 knock-out cells, highlighting the significance of BAG-1 in MCF-7[24]. In GO-Pep-treated BAG-1 knock-out MCF-7 cells, the suppression of cell survival was significantly attenuated, indicating that GO-Pep exerts its inhibitory effects primarily through its interaction with BAG-1 isoforms. This finding also suggested the selectivity of GO-Pep and minimized the possibility of its interactions with other BAG family members. Targeting BAG-1 interactions has been the subject of numerous previous attempts, starting with Thioflavin S, mixture of different compounds formed by the methylation of dehydrothio-p-toluidine. In human breast cancer cells, thioflavin S reduced the interaction of BAG-1 with Hsp70/Hsc70 and, to a lesser extent, c-Raf. Further, a Thioflavin S-derivative compound, Thio-2, N-Ethyl-4-(6-methyl-1,3-benzothiazol-2-yl)aniline, was developed and demonstrated a significant cytotoxic effect on breast cancer cells[35]. Numerous studies have been conducted regarding the effect of Thio-2 to suppress BAG-1 activity. For example, combining Thio-2 and trastuzumab has been shown to inhibit cell growth, particularly in a subclone of the SKBR3 breast cancer cell line with acquired trastuzumab resistance, implying that inhibiting BAG1 may benefit patients with HER2 positive breast cancer[36]. Thio-2 has also been reported to impede binding of BAG-1L to the androgen receptor (AR), thereby inhibiting the BAG-1L-linked AR transactivation in human prostate cancer cells[6]. Even though the efficacy of Thio-2 in cancer cells has been proven in a number of studies, it exhibited a moderate inhibition of BAG-1:HSP70 interaction which requires higher doses for treatment and a poor solubility in water. Furthermore, Thioflavin class of compounds have significant off-target effects that hinder their progress from bench to bedside[37]. Peptides, on the other hand, are more effective, selective, and safer than synthetic drugs. For this, short peptides derived from BAG-1 has been produced and shown to inhibit BAG-1:HSP70 interaction, resulting in the decrease of breast cancer cell growth[38]. Nevertheless, these studies provide the supporting evidence that BAG-1 inhibitor-anchored treatment regimens could be evaluated as a therapeutic option in cancer.

Even though GO-Pep showed promising activity on tumor cells, it is in early development stage and additional improvements to its structure are yet possible. One critical aspect is the optimization of the current formulation for in vivo studies. The systemic delivery of cationic peptides to patients with cancer might be hindered by their proteolysis and/or inactivation through negatively charged serum components. Therefore, it is important to test its stability in a biologically relevant environment. Of note, it has been reported that proteolytic stabilities of peptides vary among serum, plasma, and fresh blood for each peptide[39], potentially misleading the efforts to increase peptide stability. For enhanced stability, residues especially prone to protease cleavage can be favorably substituted to stabilize peptide sequence against proteases. Another possibility to mitigate these limitations is the use of viral expression vectors or liposomal delivery systems to deliver the peptide to tumor cells. Here, Pep3 can act as a pharmacophore template for such kind of applications. Also, to serve a lower cytotoxicity profile, Pep3 can be combined with a tumor-homing peptide[40] to specifically incorporate into tumor cells. To increase the efficacy, an Ala scanning strategy might be employed for identifying the indispensable amino acid residues of the peptide for c-Raf inhibitory activity[41]. At the present stage, we not only introduce a c-Raf-derived peptide molecule that directly binds to BAG-1 and exhibits promising anticancer properties in vitro but also provide a multi-faceted approach of investigating a significant complex from several angles. Given that this is not the finalized version of this peptide, more comprehensive mechanistic evidence will be required after future refinements to the peptide's structure and function.

Treatments that depend on a single agent often fail to efficaciously address cancer due to its genetic variability and resilience[42]. Therefore, an expanding body of evidence reveals that the sequential or synergistic inhibition of multiple effectors is a more practical route for therapeutic efficacy[12]. New inhibitors will serve as an opportunity to develop efficient and well-tolerated combinations in clinical practice. There is still room for further research on GO-Pep activity, including investigations on its anticancer effect by possible combinations with other inhibitors on targets in the Ras-signal cascade, such as B-Raf and MEK.

Methods

Antibodies

BAG-1 (#3920), c-Raf (#9422), p-c-Raf (Ser338, #9427), B-Raf (#14814), p-BRaf (Ser445, #2696), MEK1/2 (#9122), p-MEK1/2 (Ser217/221, #9121), HSP70 (#4872), Beclin 1(#3738), Akt (#9272), p-Akt (Ser473, #9271), CHIP (#2080), Vinculin (#4650), Flag (#14793). Mouse secondary antibody (#7076), Rabbit secondary antibody (#7074). All antibodies are obtained from Cell Signaling Technology. The source of all primary antibodies is rabbit except for BAG-1 (mouse).

Cell culture and transfection

HEK293T (ATCC® CRL-3216™), MCF-7 (ATCC® HTB-22™) and BEAS2b (ATCC® CRL-3588™) cells were cultured in DMEM (Dulbecco's Modified Eagle Medium, Gibco, USA) supplemented with 10% FBS (Gibco, USA) and 100U/100 $mg.ml^{-1}$ penicillin/streptomycin (Gibco, USA). SNU-387 (ATCC® CRL-2237™) and HUH-7 hepatocellular carcinoma cells were cultured in RPMI. CRISPR/Cas9-mediated BAG-1 knock-out MCF-7 cells were generated in our previous studies[24]. Cells were cultured in a 5% CO_2 incubator at 37 °C. Plasmids were diluted in serum free medium, mixed with PEI Max (Polysciences) reagent (1:3 DNA:PEI ratio) and incubated for 20 min at RT, then applied to the cells. After adding the mixture into each well, cells were cultured for about 48 h and then collected and lysed for following experiments.

Immunoblotting and TAP pull-down

Protein lysates were quantified using Bradford assay. Following protein transfer, the membrane was blocked and incubated with antibodies. Bands were visualized using ChemiDoc imaging system Bio-Rad, Richmond, CA, USA. In pull-down experiments, lysates were incubated with the IgG sepharose beads overnight at 4 °C with rotation. Samples were washed with lysis buffer and eluted with glycine-HCl (pH 2.3). Fractions were analyzed by immunoblotting. Only bead and empty vector (only TAP)-transfected cell lysates were used as negative controls.

Protein purification

His_6BAG-1S was purified as previously described[32]. 3xFlag-c-Raf overexpressing HEK293T cells were lysed in NP-40 lysis buffer supplemented with 500 mM urea and 1 mM $MgCl_2$[43]. Lysate was incubated with Anti-Flag M2 agarose affinity gel at 4 °C for 3 h. Flow-through was aspirated and resin particles were washed away. Bound protein was eluted by incubating the resin particles with 3xFlag peptide for 2 h. The purified proteins were visualized by SDS-PAGE.

Circular dichroism

Far-UV CD spectra were measured at 25 °C using a Jasco J-1500 spectropolarimeter that was set for a 190–250 nm wavelength range, 0.1 nm step resolution, 1 nm bandwidth, 0.5 s response time, and triplicate scans per sample. Samples of 2.5 μM of BAG-1S were analyzed.

Size exclusion chromatography

In a Biosuite High-resolution SEC column 250 (Waters Corp., Milford, MA), a total of 10 μg of protein was injected, and samples were processed for 25 min using an isocratic gradient. As the mobile phase, PBS (pH 7.4) was utilized. 15-600 kDa Sigma SEC standards were run under identical conditions.

HDX-MS

The experiments of HDX-MS were conducted on a Synapt G2-Si HDMS connected to an Acquity UPLC M-Class system equipped with HDX (Waters, Manchester, UK). A continuous approach was used to determine the deuterium incorporation, with labeling taking place at RT. Samples were diluted to a working concentration of 15 μM in 20 mM HEPES, 150 mM NaCl (pH 7.4). Following deuterium labeling, samples were 16-fold diluted in 20 mM HEPES, 150 mM NaCl in D_2O (pD 7.0). After various incubations, exchange was stopped at 0 °C in 20 mM HEPES, 150 mM NaCl, 3 M Guanidium-HCl, 0.2 M TCEP (pH 2.3) and then the sample was digested on-line at 20 °C using a Waters Enzymate BEH pepsin column. Further, the peptides were trapped for 3 min on a Waters BEH C18 VanGuard pre-column at a flow rate of 70 μL/min in 0.2% formic acid (pH 2.5) and transferred to a Waters BEH C-18 analytical column. The peptides were eluted at a flow rate of 40 μL/min using a linear gradient of Buffer D (0.2% formic acid in acetonitrile, pH 2.5). The chromatography and trapping steps of the experiment were carried out at 0 °C. MS data were gathered using an MS^E method in resolution mode, with lock mass correction using Leu-enkephalin after the MS was calibrated with NaI. For each protein, undeuterated reference acquisitions were made in quadruplicates, whereas labeling acquisitions of 0.2, 2, 20, and 200 min were made in triplicates The ProteinLynx Global Server (PLGS) software package was used to assign peptides, DynamX v3.0 was utilized to determine the deuterium incorporation of each assigned peptide.

Cross-linking conjugation reactions

DSS conjugation reactions were performed according to the manufacturer's procedure (21655, Thermo). C-Raf protein only or c-Raf:BAG-1S complex prepared in conjugation buffer were incubated with 2.5 mM DSS for 30 min at RT. Reactions were stopped by Laemmli buffer and samples were visualized by immunoblotting.

In vitro binding assay

BAG-1S protein was immobilized on PVDF membrane. Membranes were incubated with prey protein (3xFlagc-Raf or 3xFlagcatc-Raf) for 45 min at 37 °C, then blocked with 5% BSA and probed with BAG-1 or Flag antibody. No bait control was included as a control. Following secondary antibody treatment, membranes were visualized. To identify binder peptides, in vitro binding assay coupled to limited trypsinolysis and mass spectrometry was performed according to the previously published protocol[44]. The peptides obtained were purified and concentrated using ZipTip C18 pipette tips (Millipore), then eluted with TA30 (30:70 [v/v] acetonitrile: 0.1% TFA) and evaluated by LC-MS/MS by peptide mapping method. Peptide mapping by mass spectrometry was performed using an Acquity UPLC system coupled with a Waters Synapt G2-Si HDMS (Waters Corp). The mobile phases consisted of water (phase A), acetonitrile (ACN, phase B), and water containing 1% (v/v) formic acid (phase C). Peptides were separated on a BEH C18 reverse-phase analytical column using a gradient elution: 1–42% mobile phase B over 60 min, followed by a rapid increase to 80% B within 1 min, and an isocratic hold at 80% B for 3 min. The column was re-equilibrated for 20 min. Mobile phase C was maintained at 10% throughout the run, with a flow rate of 200 μL/min, and the column temperature was held at 65 °C. Data acquisition was conducted in MS^E mode with positive polarity ionization. Glu-fibrinopeptide B was used to calibrate the time-of-flight analyzer across a 50–2000 m/z range and served as an internal calibrant via reference spray at 30 s^{-1} intervals. Data analysis was performed using MassLynx and PLGS software (Waters Corp). No prey and no bait controls were simultaneously subjected to the same procedure.

In silico studies

For ligandibility, CavityPlus web server was utilized (http://www.pkumdl.cn:8000/cavityplus)[15]. Molecular docking was carried out using HADDOCK 2.4[45] software, using the structure of the c-Raf catalytic domain (PDB ID: 3OMV: X-Ray) and BAG-1 structure (PDB ID: 1HX1, X-Ray). Models obtained by docking were visualized using the PyMOL Molecular Graphics

System (version 2.3.1). PROtein binDIng enerGY prediction (PRODIGY) server was used for predicting the binding affinity of protein-complexes using their 3D structures[16]. Protein-Ligand Interaction Profiler (PLIP) was utilized for the identification of non-covalent interactions between interacting proteins[17]. ANCHOR web-server (http://structure.pitt.edu/anchor/) was employed for identifying the druggable binding sites in the protein-protein interaction complex[18].

MTT cell viability assay

Cells were seeded at 4×10^3 cells/well in triplicates into the 96-well plates and maintained in 100 µL high glucose DMEM media in appropriate conditions as described previously. The day after, cells were transfected with 150 ng of each N-TAP BAG-1S plasmid per well. 24, 48 and 72 h post-transfection, 10 µL of cell proliferation reagent (MTT) was added into the wells and incubated for 4 h at 37 °C and 5% CO_2. Following incubation, media was discarded and formazan crystals were dissolved in DMSO. The plate was shaken thoroughly for 1-2 min on a shaker. Subsequently, cell viability was quantified by reading absorbances against a background control as blank at 570 nm using a microplate reader. The reference wavelength was selected as 600 nm. The measurements were carried out as triplicates for each condition and cell viability was normalized to baseline and empty vector (only TAP)-transfected cells.

Synthesis and characterization of peptides

Peptides were synthesized on Rink Amide resin (CEM, Lot: RA18003) loading capacity 0.70 mmol/g as a solid support using Fmoc-based solid phase peptide synthesis. Peptide synthesis was performed with a 0.1 mmol scale with Liberty blue® (CEM, Germany) using the microwave assisted high temperature. The Fmoc protecting groups were removed by piperidine (% 20 v/v in N,N-dimethylformamide). The coupling of amino acids (0.2 M) was performed using N,N-diisopropylcarbodiimide (DIC) and ethyl-2-cyano-2-(hydroxyimino) acetate in 4 min cycle time (1 min for deprotection, 1 min for washing and 2 min for coupling) at 50 °C. For the cleavage of protecting groups, peptides were treated with 5 mL cleavage cocktail (TFA/H_2O/TIS, 95/2.5/2.5, v/v/v) for 30 min at 37 °C. The peptide was precipitated using 15 mL chilled ether by centrifugation at 3500 rpm for 5 min. The crude peptide was analyzed using RP-HPLC (Agilent Technologies 1260 Infinity) with C18 AdvanceBio Peptite Plus 2.1 × 150 mm 2.7-Micron column (Agilent Technologies) at 214 and 280 nm. Buffer A and B were water (containing 0.05% TFA) and acetonitrile (containing 0.025% TFA) respectively. Gradient for 5-80% B in 30 min, flow = 0.4 mL/min.

LC-MS/MS

Intact peptide molecular weight identification via mass spectrometry was conducted using an Acquity UPLC system coupled with a Waters Synapt G2-Si HDMS (Waters Corp). The mobile phases included water (phase A), acetonitrile (ACN, phase B), and water containing 1% (v/v) formic acid (phase C). Samples were injected onto a BEH C18 reverse-phase analytical column, with separation achieved using a gradient of 1–40% mobile phase B over 10 min, followed by a rapid increase to 80% B within 1 min, and an isocratic elution at 80% B for 3.5 min. The column was re-equilibrated over 10 min. Throughout the run, mobile phase C and flow rate were maintained at 10% and 200 µL/min, respectively, with the column temperature set to 65 °C. All analyses were performed in MS^E mode at positive polarity ionization. Glu-fibrinopeptide B was infused to calibrate the time-of-flight analyzer over a range of 50–2000 m/z and served as an internal reference spray calibrant at 30 s^{-1} intervals. Data acquisition and processing were carried out using MassLynx software (Waters Corp).

Determination of binding affinities by surface plasmon resonance

Surface Plasmon Resonance (SPR) was performed as previously described[46] using a BIAcore T200 system (Cytiva, Sweden). Anti- BAG-1 (Mouse mAb, CST) was captured on flow cell 1 and 2 to ~15 RU at flow rate, 10 µL/min for 60 s. BAG-1 protein was captured on only flow cell 2 at flow rate, 10 µL/min for 60 s. The multi-cycle kinetics method was used with the following dilutions: 0 nM, 500 nM, 1000 nM, 2000 nM, 4000 nM. Peptides were injected with 60 s association and 30 s dissociation at a flow rate of 30 µL/min through flow cell 1 and 2. Binding kinetics were calculated using BIAcore T200 Evaluation Software (version 3.2.1, Cytiva) with the 1:1 binding model.

Limited trypsinolysis

To monitor the altered stability upon complex formation, limited proteolysis was performed with trypsin digestion. BAG-1S proteins were incubated with 50-fold molar excess of Pep3 and GO-Pep separately at 37 °C for 45 min. BAG-1S proteins with or without peptides were digested with Trypsin (Promega) at 37 °C. Samples were taken at certain time points (0 min, 1.5 min, 5 min, 10 min, 15 min, 45 min, 90 min). Reaction was quenched with 4X Laemmli buffer and samples were analyzed by immunoblotting. Data were analyzed by normalizing values to 0 min.

Apoptosis assay

Annexin-V staining was performed according to the protocol of Elabscience Apoptosis detection kit (cat no: E-CK-A214). Cancer cells (1.0×10^5 cells/mL) were suspended in serum-free medium and incubated with the respective compound in 6-well plates in a CO_2 incubator. Two different doses including 25 µM and 50 µM were administered to MCF-7 cells. After treatment with compounds for 48 h, the cancer cells were harvested and incubated with APC-Annexin V and 7-AAD.

Colony formation

The cells were seeded at a density of 300 cells/well (for MCF-7) in 3 mL complete culture medium. GO-Pep were applied to the cells for 48 h (50 µM or 100 µM). Then the old medium was removed, and new fresh complete medium was added to the cells. After two weeks, the colonies formed were dyed with methylene blue solution (50% methanol, 50% distilled water, and 0.4 g methylene blue) and counted using ImageJ 1.53a software (NIH, USA). The differences between the groups were analyzed with Prism v8.

Flow cytometry

Annexin-V staining was performed according to the protocol of Elabscience Apoptosis detection kit (cat no: E-CK-A214). Cancer cells (1.0×10^5 cells/mL) were suspended in serum-free medium and incubated with the respective compound in 6-well plates in a CO_2 incubator. Two different doses including 25 µM and 50 µM were administered to MCF-7 cells. After treatment with compounds for 48 h, the cancer cells were harvested and centrifuged, then incubated with Annexin V and 7AAD. The fluorescence emission was detected at 633 nm. After incubation of results were shown in 4 different groups in the dot plot: lower left quadrant, living cells (Annexin V-/7AAD −); lower right quadrant, early apoptotic cells (Annexin V + /7AAD −); upper left quadrant, necrotic cells (Annexin V − /7AAD +); upper right quadrant, late apoptotic cells (Annexin V + /7AAD +). Gate strategy was given in Fig. S6.

Statistics and reproducibility

Experiments were conducted as independent replicates. The effect of BAG-1S mutations on MAPK pathway was evaluated using biological triplicates. In vitro binding experiments were performed as two biological replicates. Limited trypsinolysis experiments were done as singlets to complement in vitro binding experiments. The experiments regarding to the cellular effect of GO-Pep on MCF-7 cells were carried out as biological duplicates. When applicable, orthogonal or complementary methods were adopted to reduce bias. Cell viability values are the normalized mean values of technical triplicates. Quantifications was carried out by densitometry analysis utilizing ImageJ software (version 1.52a) with the same parameters. Quantitative data are represented as mean ± standard deviation. To build all graphs, Graphpad Prism 10 was used. Statistical significance was assessed using P values calculated via an unpaired two-tailed Student's t-test. Statistical significance was ascribed to differences where $P \leq 0.05$ (*), $P \leq 0.01$ (**), or $P \leq 0.001$ (***).

Reporting summary

Further information on research design is available in the Nature Portfolio Reporting Summary linked to this article.

Data availability

Uncropped western blots are provided in Supplementary Information. The source data underlying the graphs and HDX summary table can be found in the Supplementary Data. The mass spectrometry data have been deposited to the deposited to the PRoteomics IDEntification (PRIDE)[47] Database with the dataset identifier PXD058656.

Received: 9 July 2024; Accepted: 18 December 2024;
Published online: 28 February 2025

References

1. Papadakis, E. S. et al. BAG-1 as a biomarker in early breast cancer prognosis: A systematic review with meta-analyses. *Br. J. Cancer* **116**, 1585–1594 (2017).
2. Ni, W. et al. Overexpressed nuclear BAG-1 in human hepatocellular carcinoma is associated with poor prognosis and resistance to doxorubicin. *J. Cell Biochem* **114**, 2120–2130 (2013).
3. Mariotto, E. et al. BAG1 down-regulation increases chemo-sensitivity of acute lymphoblastic leukaemia cells. *J. Cell Mol. Med* **25**, 9060 (2021).
4. Götz, R., Kramer, B. W., Camarero, G. & Rapp, U. R. BAG-1 haplo-insufficiency impairs lung tumorigenesis. *BMC Cancer* **4**, 1–6 (2004).
5. Wang, Y. et al. BAG-1L protects SH-SY5Y neuroblastoma cells against hypoxia/re-oxygenation through up-regulating HSP70 and activating PI3K/AKT signaling pathway. *Neurochem. Res.* **42**, 2861–2868 (2017).
6. Cato, L. et al. Development of bag-1L as a therapeutic target in androgen receptor-dependent prostate cancer. *Elife* **6**, e27159 (2017).
7. Mariotto, E., Viola, G., Zanon, C. & Aveic, S. A BAG's life: Every connection matters in cancer. *Pharmacol Ther.* **209**, 107498 (2020).
8. Liu, S. et al. Over-expression of BAG-1 in head and neck squamous cell carcinomas (HNSCC) is associated with cisplatin-resistance. *J. Transl. Med.* **15**, 1–11 (2017).
9. Kilbas, P. O., Akcay, I. M., Doganay, G. D. & Arisan, E. D. Bag-1 silencing enhanced chemotherapeutic drug-induced apoptosis in MCF-7 breast cancer cells affecting PI3K/Akt/mTOR and MAPK signaling pathways. *Mol. Biol. Rep.* **46**, 847–860 (2019).
10. Yang, X. et al. Human BAG-1/RAP46 protein is generated as four isoforms by alternative translation initiation and overexpressed in cancer cells. *Oncogene* **17**, 981–989 (1998).
11. Song, J., Takeda, M. & Morimoto, R. I. Bag1-Hsp70 mediates a physiological stress signalling pathway that regulates Raf-1/ERK and cell growth. *Nat. Cell Biol.* **3**, 276–282 (2001).
12. Tatli, O. & Doganay, G. D. Recent developments in targeting RAS downstream effectors for RAS-driven cancer therapy. *Molecules* **26**, (2021).
13. Wu, P. et al. Overexpression of Raf-1 in basal-like carcinoma of the breast: Correlation with clinicopathology and prognosis. *Contemp. Oncol.* **18**, 391 (2014).
14. Riaud, M. et al. The role of CRAF in cancer progression: From molecular mechanisms to precision therapies. *Nat. Rev. Cancer 2024* 1–18, https://doi.org/10.1038/s41568-023-00650-x (2024).
15. Wang, S., Xie, J., Pei, J. & Lai, L. CavityPlus 2022 update: An integrated platform for comprehensive protein cavity detection and property analyses with user-friendly tools and cavity databases. *J. Mol. Biol.* **435**, 168141 (2023).
16. Xue, L. C., Rodrigues, J. P., Kastritis, P. L., Bonvin, A. M. & Vangone, A. PRODIGY: A web server for predicting the binding affinity of protein-protein complexes. *Bioinformatics* **32**, 3676–3678 (2016).
17. Adasme, M. F. et al. PLIP 2021: Expanding the scope of the protein-ligand interaction profiler to DNA and RNA. *Nucleic Acids Res.* **49**, W530–W534 (2021).
18. Meireles, L. M. C., Dömling, A. S. & Camacho, C. J. ANCHOR: A web server and database for analysis of protein–protein interaction binding pockets for drug discovery. *Nucleic Acids Res*. **38**, W407 (2010).
19. Turk, M. et al. Co-chaperone bag-1 plays a role in the autophagy-dependent cell survival through beclin 1 interaction. *Molecules* **26**, 854 (2021).
20. Lipinski, C. A., Lombardo, F., Dominy, B. W. & Feeney, P. J. Experimental and computational approaches to estimate solubility and permeability in drug discovery and development settings. *Adv. Drug Deliv. Rev.* **46**, 3–26 (2001).
21. Hao, M., Zhang, L. & Chen, P. Membrane internalization mechanisms and design strategies of arginine-rich cell-penetrating peptides. *Int. J. Mol. Sci.* **23**, 9038 (2022).
22. de Oliveira, E. C. L. et al. Predicting cell-penetrating peptides using machine learning algorithms and navigating in their chemical space. *Sci. Rep.* **11**, 1–15 (2021).
23. Alland, C. et al. RPBS: A web resource for structural bioinformatics. *Nucleic Acids Res.* **33**, W44–W49 (2005).
24. Kilbas, P. O. et al. CRISPR/Cas9-mediated Bag-1 knockout increased mesenchymal characteristics of MCF-7 cells via Akt hyperactivation-mediated actin cytoskeleton remodeling. *PLoS One* **17**, e0261062 (2022).
25. Karreth, F. A., Frese, K. K., DeNicola, G. M., Baccarini, M. & Tuveson, D. A. C-Raf is required for the initiation of lung cancer by K-Ras(G12D). *Cancer Discov.* **1**, 128–136 (2011).
26. Sanclemente, M. et al. c-RAF ablation induces regression of advanced Kras/Trp53 mutant lung adenocarcinomas by a mechanism independent of MAPK signaling. *Cancer Cell* **33**, 217–228.e4 (2018).
27. Dumaz, N. et al. In melanoma, RAS mutations are accompanied by switching signaling from BRAF to CRAF and disrupted cyclic AMP signaling. *Cancer Res.* **66**, 9483–9491 (2006).
28. Zhang, K. et al. Overexpression of Raf-1 and ERK1/2 in sacral chordoma and association with tumor recurrence. *Int. J. Clin. Exp. Pathol.* **8**, 608 (2015).
29. Xie, X., Clausen, O. P. F. & Boysen, M. Bag-1 expression as a prognostic factor in tongue squamous cell carcinomas. *Laryngoscope* **114**, 1785–1790 (2004).
30. Noguchi, T. et al. Nuclear BAG-1 expression is a biomarker of poor prognosis in esophageal squamous cell carcinoma. *Dis. Esophagus* **16**, 107–111 (2003).
31. Gennaro, V. J., Wedegaertner, H. & McMahon, S. B. Interaction between the BAG1S isoform and HSP70 mediates the stability of anti-apoptotic proteins and the survival of osteosarcoma cells expressing oncogenic MYC. *BMC Cancer* **19**, 1–14 (2019).
32. Can, N. D. et al. Interactome analysis of Bag-1 isoforms reveals novel interaction partners in endoplasmic reticulum-associated degradation. *PLoS One* **16**, e0256640 (2021).
33. Pan, M. et al. Identification of an imidazopyridine-based compound as an oral selective estrogen receptor degrader for breast cancer therapy. *Cancer Res. Commun.* **3**, 1378–1396 (2023).
34. Maddalo, D. et al. A peptidic unconjugated GRP78/BiP ligand modulates the unfolded protein response and induces prostate cancer cell death. *PLoS One* **7**, e45690 (2012).
35. Enthammer, M. et al. Isolation of a novel thioflavin S-derived compound that inhibits BAG-1-mediated protein interactions and targets BRAF inhibitor-resistant cell lines. *Mol. Cancer Ther.* **12**, 2400–2414 (2013).
36. Papadakis, E. et al. A combination of trastuzumab and BAG-1 inhibition synergistically targets HER2 positive breast cancer cells. *Oncotarget* **7**, 18851–18864 (2016).
37. Chakraborty, M., Jin, K. J., Glover, S. A. & Novak, M. Characterization of the 4-(Benzothiazol-2-yl)phenylnitrenium ion from a putative metabolite of a model antitumor drug. *J. Org. Chem.* **75**, 5296–5304 (2010).
38. Sharp, A., Cutress, R. I., Johnson, P. W. M., Packham, G. & Townsend, P. A. Short peptides derived from the BAG-1 C-terminus inhibit the

interaction between BAG-1 and HSC70 and decrease breast cancer cell growth. *FEBS Lett.* **583**, 3405–3411 (2009).
39. Boöttger, R., Hoffmann, R. & Knappe, D. Differential stability of therapeutic peptides with different proteolytic cleavage sites in blood, plasma and serum. *PLoS One* **12**, e0178943 (2017).
40. Kondo, E., Iioka, H. & Saito, K. Tumor-homing peptide and its utility for advanced cancer medicine. *Cancer Sci.* **112**, 2118–2125 (2021).
41. Niida, A. et al. Investigation of the structural requirements of K-Ras(G12D) selective inhibitory peptide KRpep-2d using alanine scans and cysteine bridging. *Bioorg. Med. Chem. Lett.* **27**, 2757–2761 (2017).
42. Vasan, N., Baselga, J. & Hyman, D. M. A view on drug resistance in cancer. *Nature* **575**, 299–309 (2019).
43. Kondo, Y. et al. Cryo-EM structure of a dimeric B-Raf:14-3-3 complex reveals asymmetry in the active sites of B-Raf kinases. *Science* **366**, 109–115 (2019).
44. Mertinková, P. et al. A simple and rapid pipeline for identification of receptor-binding sites on the surface proteins of pathogens. *Sci. Rep.* **10**, 1–13 (2020).
45. Honorato, R. V. et al. Structural biology in the clouds: The WeNMR-EOSC ecosystem. *Front Mol. Biosci.* **8**, 729513 (2021).
46. Mahmoudi Azar, L. et al. Expression and characterization of recombinant IL-1Ra in Aspergillus oryzae as a system. *BMC Biotechnol.* **23**, 1–15 (2023).
47. Perez-Riverol, Y. et al. The PRIDE database at 20 years: 2025 update. *Nucleic Acids Res.* **53**, D543–D553, https://doi.org/10.1093/nar/gkae1011 (2024).

Acknowledgements

This study is supported by the Scientific & Technological Research Council of Türkiye (TUBITAK) 1001 program [Grant number: 117Z848].

Author contributions

Conceptualization: O.T., G.D.D., Methodology: O.T., E.C., M.T., A.S., B.D., B.Z.T., A.E.E., B.B., Investigation: O.T., E.B., Visualization: O.T., E.E., B.E., O.C., G.D.D., Funding acquisition: G.D.D., Supervision: G.D.D., Writing—original draft: O.T., Writing—review & editing: E.E., B.E., O.C., G.D.D.

Competing interests

This article is related to a patent application filed at the Turkish Patent Office under the number of 2023/010146 (PCT/TR2024/050975). O.T and G.D.D. have been listed as inventors on patent applications for the inhibitors. The authors declare no other conflicts of interest.

Additional information

Supplementary information The online version contains supplementary material available at https://doi.org/10.1038/s42003-024-07419-4.

Correspondence and requests for materials should be addressed to Gizem Dinler Doganay.

Peer review information *Communications Biology* thanks Andrew Cato, Elena Mariotto and Adam Sharp for their contribution to the peer review of this work. Primary Handling Editors: Ross Bathgate and Laura Rodríguez Pérez.